Title

THE A-HYPERON MASS AND ENERGY SPECTRUM FROM THE NUCLEAR CAPTURE OP NEGATIVE K MESONS

Author

Mason, Conrad J.

Publication Date

1960-07-01

UCRL 9297

UNIVERSITY OF
CALIFORNIA

Ernest O. Lawrence

Radiation Laboratory

THE Λ-HYPERON MASS AND ENERGY SPECTRUM FROM THE NUCLEAR CAPTURE OF NEGATIVE K MESONS

DISCLAIMER

UCRL-9297
UC-34 Physics and Mathematics
TID-4500 (15th Ed.)

UNIVERSITY OF CALIFORNIA

Lawrence Radiation Laboratory
Berkeley, California

Contract No. W-7405-eng-48

THE Λ-HYPERON MASS AND ENERGY SPECTRUM FROM THE NUCLEAR CAPTURE OF NEGATIVE K MESONS

Conrad J. Mason

(Thesis)

July 7, 1960

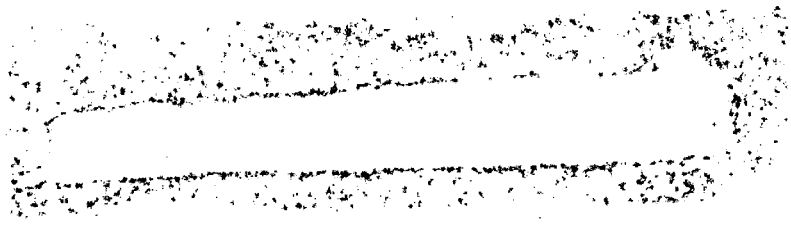

Printed in USA. Price $1.25. Available from the
Office of Technical Services
U. S. Department of Commerce
Washington 25, D.C.

THE Λ-HYPERON MASS AND ENERGY SPECTRUM FROM THE NUCLEAR CAPTURE OF NEGATIVE K MESONS

Contents

Abstract 3

Introduction 4

Experimental Arrangement

2B Stack 7

2D Stack 10

Scanning Procedure 13

Measurements

Range 14

Shrinkage Factor 16

Emulsion Density 17

Angles 20

Calculations

Range 21

Space Angle 23

Mass and Q Value 24

Energy Spectrum 31

Acknowledgments 39

Appendix

Automated Microscope 40

References 48

THE Λ-HYPERON MASS AND ENERGY SPECTRUM FROM THE NUCLEAR CAPTURE OF NEGATIVE K MESONS

Conrad J. Mason

Lawrence Radiation Laboratory
University of California
Berkeley, California

July 7, 1960

ABSTRACT

In two emulsion stacks exposed to K^--meson beams, a total of 128 Λ-like decays in which the secondaries came to rest were found by area scanning in the region of stopping K mesons. All of these events were analyzed and 116 proved to be hyperons. The range-measurement techniques employed were essentially those used by Barkas and co-workers in determining the range-energy relation for emulsion. The emulsion densities and shrinkage factors were precisely determined in order to obtain reliable results. The Λ-hyperon mass as obtained from the analysis of the events in the first stack is 1115.30±0.11 Mev (29 events); in the second, it is 1115.46±0.09 Mev (87 events). The errors include the statistical and systematic errors associated with each stack. The two mass values are not inconsistent. The weighted mean mass is 1115.40±0.14 Mev, where the total error arises from the statistical errors of the two determinations and from an 0.12-Mev error associated with systematic effects, i.e., the error in the range-energy relation and the uncertainties in the rest masses of the secondaries. The corresponding Q value for the decay via the charged mode is 37.56±0.13 Mev. The Λ-hyperon production spectrum from the capture of K^- mesons is presented. A description of a microscope equipped with automatic coordinate-readout devices is appended.

INTRODUCTION

The original observations of unstable particles of transnucleonic mass arising from the interaction of cosmic radiation with matter, have led to many attempts to determine the fundamental properties of these particles. Among the first to be investigated was the Λ-hyperon, a neutral particle whose decay into two charged secondaries gives rise to a characteristic V-shaped event. In 1947, such a decay was first observed in a cloud chamber by Rochester and Butler.[1] Subsequent observations of similar events by others led to the identification of the secondaries as a proton and a pion.

Once the decay mode was established, it became possible to determine the Q value of the decay and, consequently, the Λ-hyperon mass. Early cloud chamber experiments to determine the Q value were hampered by a scarcity of events, since Λ-hyperons were observed only infrequently. The rarity of events, coupled with systematic errors inherent in cloud chamber measurements, rendered impossible a precise mass determination. Results of these early experiments are presented in a review article by R. W. Thompson.[2] In an effort to reduce the magnitude of systematic errors, Friedlander et al. in 1954 employed nuclear track emulsion exposed to cosmic radiation; on the basis of ten events, they found the Q value to be 36.92 ± 0.22 Mev, a result consistent with the cloud chamber measurements.[3]

Danysz and Pniewski in 1952 discovered in emulsion a star-producing fragment from a high-energy cosmic-ray interaction, a finding which led to the proposal that such a nuclear "hyperfragment" contains a bound hyperon.[4] Of necessity, only a Λ-hyperon can remain bound long enough for the fragment to be observable; a Σ^0 hyperon decays via γ emission almost immediately into a Λ-hyperon, whereas fast reactions producing Λ-hyperons occur for $\Sigma^{\pm}$ hyperons. The experimental verification of the above hypothesis is dependent upon the measurement of a positive binding energy for the Λ-hyperon in a hyperfragment.

A survey of hyperfragment binding energies presented at the 1957 Rochester conference by Telegdi,[5] in which he used the above emulsion value for the Q value of the Λ-hyperon decay, showed negative binding energies for hyperfragments tentatively identified as either ${}_{\Lambda}H^{2}$ or ${}_{\Lambda}H^{3}$. A grouping of these uncertain events with those definitely identified as ${}_{\Lambda}H^{3}$ still showed an over-all net deficit in binding energy of approximately 0.12 Mev. Yet, clearly, ${}_{\Lambda}H^{3}$ hyperfragments did exist. This situation was untenable, and one had either to invalidate the assumption that a bound hyperon was present or to attribute a systematic error to the Q-value measurement. Because the remaining hyperfragments did exhibit positive binding energies--which seemed to suggest the correctness of the hypothesis, supported also by evidence from hyperfragment decay modes--a remeasurement of the Λ-hyperon mass was in order. A cloud chamber Q-value measurement by D'Andlau et al. of 37.9±0.4 Mev was also presented at this conference.[6]

The concurrent development of large accelerators, notably the Cosmotron and Bevatron, and of beam-separation techniques had permitted production of "copious" quantities of strange particles. At Berkeley, Barkas et al. had developed an enriched K^{-}-meson beam that was utilized to expose a series of emulsion stacks.[7] These stacks contained large numbers of hyperons resulting from K^{-}-meson reactions with nuclei of the emulsion. To redetermine the mass of the Λ-hyperon, one stack--the 2B stack--was scanned for Λ-hyperon decays. Preliminary results of the analysis of these decays were presented at the Padua-Venice Conference in 1957.[8] On the basis of 18 events, we found the Q value to be 37.45±0.17 Mev, a sufficient increase over the previous emulsion measurement to give the ${}_{\Lambda}H^{3}$ hyperfragments a positive binding energy.

Our result, although in accord with the cloud chamber measurement by D' Andlau et al., was clearly at variance with the hitherto accepted Q value. Subsequent emulsion studies have given results not in disagreement with our preliminary value. Bogdanowicz et al. have reported a Q value of 37.58±0.18 Mev on the basis of 53 events.[9] Also, Brucker et al. have found a value of 37.71±0.16 Mev, as quoted by Ammar et al. in a recently completed survey of hyperfragment binding energies.[10]

The final result of our mass determination is presented here. This study incorporates 92 events found in a second stack--the 2D stack--exposed to a K^--meson beam separated by a coaxial velocity spectrometer, 11 2B stack events not included in our preliminary study, and the previously published data.

The kinematic analysis of a Λ-hyperon decay yields not only a mass value but also the kinetic energy of the hyperon at its decay point. Consequently, by applying suitable corrections to the observed energy spectrum as constructed from such decays, the energy spectrum of the Λ-hyperons at production may be obtained. These corrections--whose primary purpose is to take into account the geometry of the experiment--have been applied to the energy spectrum of the Λ-hyperons observed in the 2D stack, and the corrected spectrum is presented. One can also evaluate the absolute yield of Λ-hyperons ultimately produced as a result of K^--meson captures by the nuclei of the emulsion if (a) a sufficient number of events can be included to limit statistical errors to reasonable values, and (b) reliable data on scanning efficiencies and biases are obtained. Because these conditions could not be met in this experiment, any attempt to determine a meaningful value for the yield would prove fruitless.

A description of a microscope equipped with automatic coordinate-readout devices is appended. This instrument was employed to facilitate the range measurements.

EXPERIMENTAL ARRANGEMENT

2B Stack

Consisting of 240 600-micron pellicles of Ilford G.5 nuclear track emulsion, the 2B stack when assembled was 12 inches long, 9 in. wide, and 6 in. high. It was exposed to a 300-Mev/c separated K^--meson beam. The experimental arrangement of the apparatus used to develop the beam and the location of the stack at exposure are illustrated in Fig. 1. The 6.2-Bev proton beam of the Bevatron is allowed to strike a 1/2 X1X3-1/2-in. copper flip-up target at the 73-deg position near the north tangent tank. Negatively charged secondary particles in the forward direction relative to the primary beam are deflected outwards by the magnetic field of the Bevatron. Of these secondaries, only those having momenta in the interval 435±20 Mev/c can pass through the collimating slit formed by the yoke of the Bevatron magnet. At the point of exit from the Bevatron structure, the particles have a central momentum of 427 Mev/c; this difference in momentum is caused by energy loss in the wall of the vacuum tank. The beam flux here is of the order of 6×10^3 particles per cm^2 per 10^{13} protons on the target, with a π^-/K^- ratio of 3000/1. After passing through the quadrupole focusing magnet, the beam traverses a polyethylene degrader (nominal thickness 19.4 g/cm^2), which reduces the π^- momentum to 394 Mev/c, and the K^- momentum to 300 Mev/c. The analyzing magnet in the system serves to separate these two beam components spatially, the final separation between the peaks being approximately 19 in., with the K^- mesons undergoing a deflection of nearly 180 deg. At the stack position, the K^--meson flux is 50 $K^-/cm^2/10^{13}$ p on the target, the ratio of minimum-ionizing tracks to K mesons being $\approx$ 800/1, with a momentum gradient of 1.6 Mev/c/cm along the face of the stack and a momentum dispersion of ±2%.

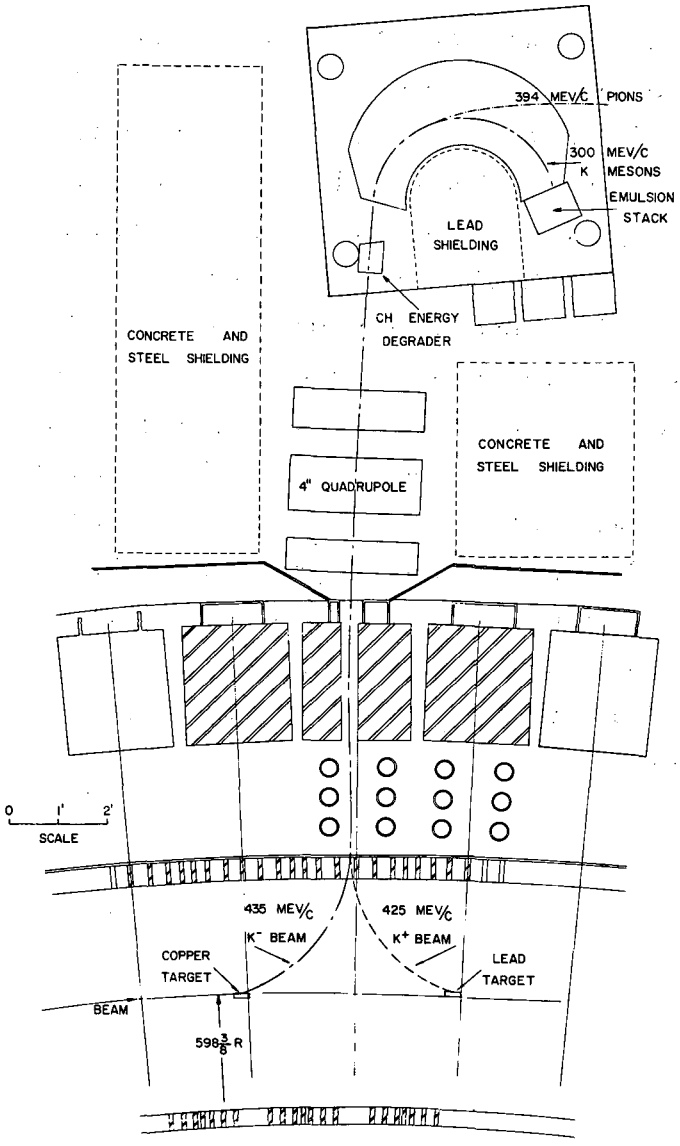

Fig. 1. Experimental arrangement of the separated K^- beam for the 2B stack exposure.

The stack was exposed with the pellicles in the horizontal plane, the K mesons incident upon the 12×6-in. face of the stack. During the course of the exposure--for which a total of 7×10^{13} protons were incident on the target--the stack position was altered by successive elevations, giving it a nearly uniform exposure. The background components of the K beam, all of which were minimum-ionizing, consisted of μ mesons (arising from π-meson decay between the target and detector), electrons, and pions, in a ratio of 8/1/1. It was hoped that the final analyzing magnet would effect a complete separation of the π^--meson and K^--meson beams; its failure to do so can be attributed to scattering in the shielding, degrader, and Bevatron magnet structure, as well as to the presence of secondary pion sources. However, of the twice-minimum tracks entering the stack within 10 deg of the expected beam direction, approximately 95% are K^- mesons. Since μ mesons are weakly interacting particles, their presence in large numbers did not hinder scanning for Λ-like events. On the other hand, the π flux from all sources produced background that seriously hampered such scanning.

2D Stack

The 2D stack, composed of 108 3×6-in. pellicles, 600 μ thick, of Ilford K.5 nuclear track emulsion, was exposed to a K^--meson beam separated by a coaxial velocity spectrometer.[11] A schematic diagram illustrating the experimental arrangement for this exposure is given in Fig. 2. The secondary beam was produced and extracted in much the same manner as for the 2B-stack exposure, with the exception that a slightly smaller (3¬1/2×1/2×1/2-in) copper flip target was used. In addition, a new beam port was channeled through the magnet structure in which was placed a 40-in. 1/4-mil polyethylene bag filled with helium to reduce multiple scattering of the secondary beam over this portion of its path. The central momentum of the beam at the point of exit from the Bevatron was 450 Mev/c.

A detailed description of the beam optics and apparatus is given by Horwitz, et al.,[12] who developed the beam. The front face of the stack was placed 6 in. behind the 1×1/2-in. aperture of collimator C2, with the pellicles in the vertical plane. The orientation was such that the K mesons entered parallel to the 6-in. axis of the stack, as shown in Fig. 3, which also depicts the beam geometry at the stack position. The front face was shielded from x rays by 1/4-in. Pb, the remaining faces shielded by Pb, Cd, and paraffin. At the stack location the ratio of minimum-ionizing tracks to K mesons was 100/1, with a K flux of approx 20 $K^-/cm^2/10^{13}$ p on the target. The exposure time was such that 1.3×10^{14} protons were incident on the target. Approximately 85% of the background consisted of μ mesons, and possibly electrons, the remaining 15% being π mesons. From the range distribution of the K mesons, one finds the K-meson momentum at stack entry to be 430±10 Mev/c.

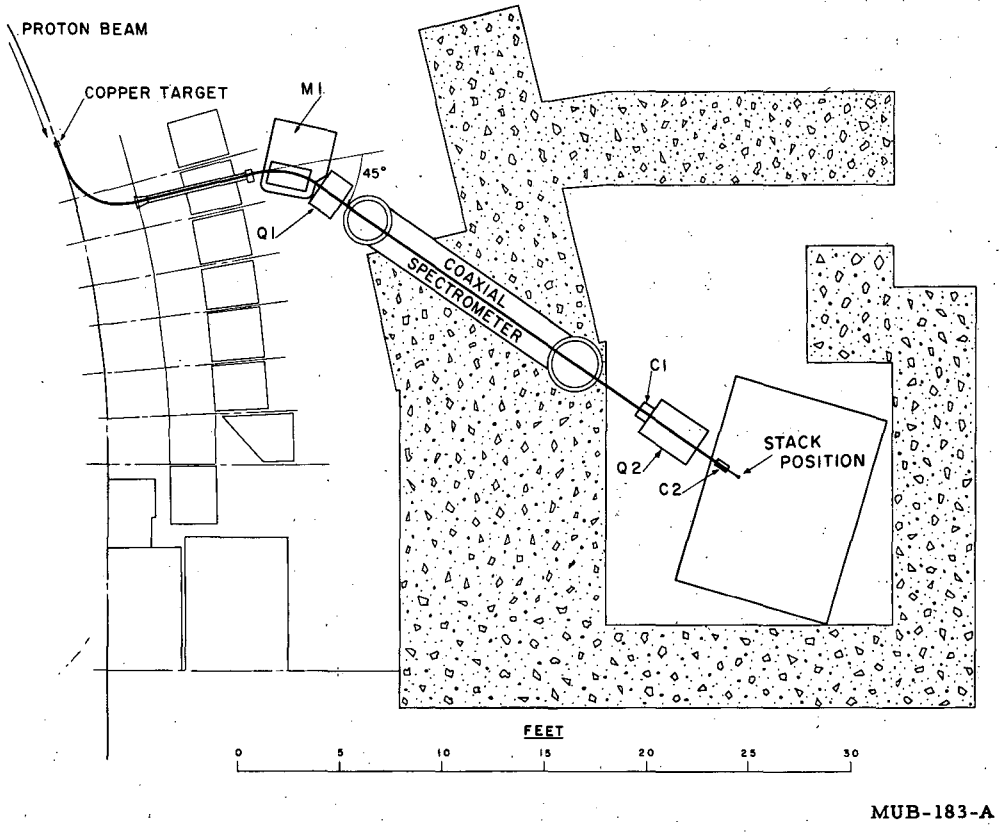

Fig. 2. Experimental arrangement of the separated K^- beam for the 2D stack exposure. The stack was placed 6 in. behind the aperture of Collimator C2.

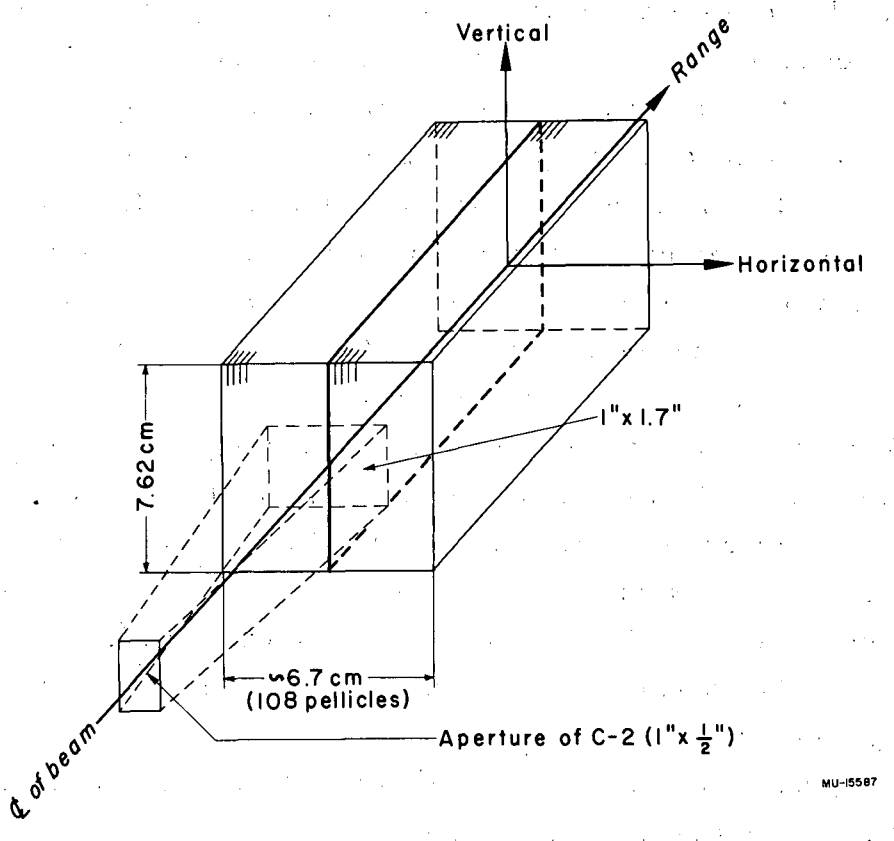

Fig. 3. Beam geometry at the stack position for the 2D stack exposure.

SCANNING PROCEDURE

In both the 2B and 2D stacks, the events corresponding to Λ-hyperon decays were located by area-scanning the region in which the K^- mesons came to rest. The following criteria were established to aid in the identification of Λ-like events:

1. The origin of the event must be "clean," i.e., characterized by the absence of any grain or grains indicative of an interaction.

2. An increase in grain density of both tracks must be observed as each is followed outward from the origin. An exception is a short dark track, in which it is impossible to detect such a change.

3. The tracks must have the proper terminal behavior for their supposed identities, e.g., a track tentatively identified as a pion should show the characteristic scattering for this particle near the end of its range as well as an indication of a terminal interaction.

Scanning a total volume of 160 cm^3 in the 2B stack yielded 35 Λ-like events which satisfied the above criteria. For the 2D stack, 92 similar events were found in a scanned volume of 50 cm^3.

The scanning efficiencies for locating Λ-like events are markedly different for the two stacks. Because of the relatively large amount of background present in the 2B stack, the average scanning efficiency is $\approx$15%. On the other hand, for the 2D stack this figure is $\approx$41 %.

Only those Λ-like events whose secondaries came to rest were used in the mass determination. Although it is possible to determine the residual range of a particle that interacts in flight by means of grain- or blob-counting techniques or both, the uncertainty in this quantity is such as to preclude obtaining precise results when applied to a mass determination.

MEASUREMENTS

Range

In order to be utilized as an instrument for precision range measurements in nuclear track emulsion, a microscope must have three coordinate axes, each equipped with some form of readout device to measure length. The X and Y axes are usually defined by precision lead screws which provide for translation of the stage in two directions, the Z axis being defined by the optic axis of the microscope. The measure of length in this last direction is the displacement of the objective necessary to keep a track in focus as it is being followed. The range of a particle is measured with respect to the coordinate system formed by these three axes.

All range measurements were performed on the automated microscope described in the appendix, except for ranges < 1 mm. Periodicity in microscope lead screws does not permit precise measurement of such short ranges; instead, as a substitute, a calibrated reticle is employed. Microscopes were equipped with 10X oculars and 53X oil-immersion objectives for the range measurements.

Owing to the multiple scattering of a particle as it traverses a medium, a measurement of its true range cannot be obtained. Instead, the trajectory must be approximated by a series of straight-line segments whose end points are selected by a predetermined convention. Here, the convention adopted is that which was used by Barkas et al.[13] to establish the range-energy relation in emulsion, i.e., the three coordinates of the track are recorded whenever the particle undergoes a single scattering ≥ 5 deg or when the total scattering accumulated since the previous measurement is 5 deg. Such a rectification of the path of the particle results in a measured range in error by $<0.1\%$ of the true range, and introduces no error in the determination of particle energy, this energy being found from the range-energy relation.

The range of each track was measured independently by two observers. The average difference in the two results is <0.7%. Because range straggle for the pion and the proton is of the order of 3% and 1% respectively, this degree of precision in the range measurements was deemed adequate.

Shrinkage Factor

When nuclear track emulsion undergoes processing, a contraction in the vertical dimension occurs. Naturally one is interested in the range of a particle in the unprocessed emulsion. Accordingly, a correction factor must be introduced which multiples all vertical dimensions. Further, even after processing, the thickness of any pellicle is not constant, but depends upon the relative humidity. The use of a shrinkage factor makes the necessary corrections for both these effects.

Prior to processing, a sample of pellicles is taken from the stack. The thicknesses of these pellicles are measured, either directly or as a by-product of determining their densities. After the processing, the thicknesses of these pellicles are remeasured at a standard reference point; the shrinkage factor for the prevailing relative humidity is defined as the mean ratio of the unprocessed to the processed thickness. Concurrently, the thicknesses of the other pellicles of the stack are determined at the reference point. It is assumed that the shrinkage factor obtained from the sample applies to these pellicles also, since the magnitude of the shrinkage is determined primarily by the glycerin concentration of the final alcohol drying bath. For a group of pellicles processed in a single batch, the shrinkage factor is reasonably constant, enabling one to obtain the original thickness of each pellicle.

By utilization of the techniques outlined above, the shrinkage factors for both stacks were determined to ±1%.

To allow for the change in shrinkage factor caused by fluctuations in the relative humidity, the following procedure is adopted: Before any measurements are taken in a particular pellicle, its thickness is determined at the reference point. Comparison of this value with the original allows an evaluation of an "instantaneous" shrinkage factor to be applied in the subsequent range calculations.

Emulsion Density

Variation of emulsion density occurs primarily because of the absorption of water vapor. Since the stopping power of water is quite different from that of dry emulsion, there is a marked dependence of stopping power upon density. The nonlinear nature of this dependence is illustrated by Fig. 4, in which the percent range decrease per percent density increase is plotted as a function of particle velocity.[13] In order that the needed range corrections may be applied, one must evaluate the emulsion density, preferably in such a manner that the density measured is that which the emulsion possessed at the time of exposure.

A precise determination of the emulsion density is perhaps best made by an application of Archimedes' principle to successive weighings of emulsion samples in air and in carbon tetrachloride. For large pellicles, as in the 2B stack, these samples were obtained by cutting off unimportant portions of the pellicles. In the 2D stack, on the other hand, entire pellicles served as samples. Weighing the entire pellicle seems the more reliable procedure, since it minimizes the error introduced by changes in density near pellicle edges.

By the above procedure, the emulsion densities of the two stacks used in this experiment were determined to ±0.1%. As the 2B stack was composed of several manufacturer's batches, care was taken to insure the selection of several emulsion samples from each batch. Further, after assembly, the stacks were not dismantled until processing was initiated, at which time the density measurements were taken. This procedure insures that the measured density at the time of measurement is the same as the density of the stack at the time of exposure. The density measurements appear in Table I.

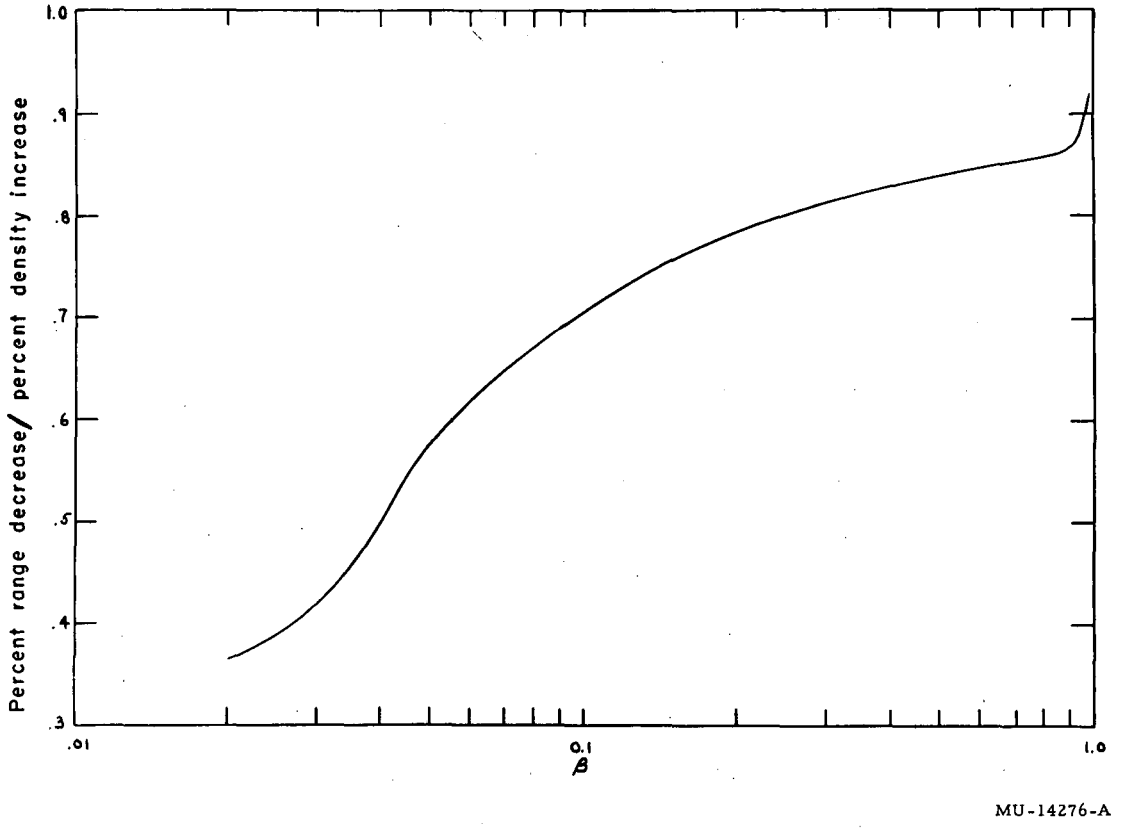

Fig. 4. Variation of proton range with emulsion density. The percent range decrease per percent density increase above the standard density of 3.815 g/cc is plotted against the velocity (β) of the particle.

Table I

Measured emulsion densities

Stack	Batch densities (g/cc)	Mean density (g/cc)
2B	3.8212±0.0010	3.8258±0.0046
	3.8303±0.0015	
2D	3.8392±0.0029	.....

Because of the manner in which the 2B stack was assembled, successive pellicles were not from the same batch. The figure quoted in the last column of Table I is the mean density as calculated from those batch densities represented in the central portion of the stack, the region in which the Λ-decay secondaries were observed and measured. The error given is the internal standard deviation of the mean. It is this mean value which was used in calculating the 2B-stack range corrections.

Determining emulsion density in the above manner allows one to find the volume of the samples used. If, in particular, these samples are entire pellicles, their areas can be measured after processing. Since they are mounted on glass, shrinkage in the transverse dimensions is negligible. Thus, for each pellicle, the ratio of volume to area equals its mean unprocessed thickness, a quantity which can be utilized in finding the shrinkage factor.

Angles

In order to determine the space angle between the secondaries of the Λ-hyperon decay, one must measure (a) the projection of the space angle in the horizontal plane (normally, the plane of the emulsion), and (b) the inclinations of the secondaries with respect to the horizontal, i.e., the dip angles.

The projected angle is found with the aid of a hairline reticle mounted in the focal plane of the microscope ocular, which, in turn, is clamped to a goniometer affixed to the eye tube. Particular attention was paid to the problem of determining the true track direction. Erroneous measurements may result from small-angle scatterings of the secondary near the origin of the event. In lieu of a rigid convention, the shortest length of track consistent with obtaining a reliable measurement was used. With two independent observations made of each event, the projected angle was found to have an uncertainty of ±0.2 deg.

The dip angle of a particular track is obtained by measuring its vertical displacement after it has traversed a known horizontal distance. A calibrated reticle in the microscope ocular is used to establish the horizontal distance, and the fine-focus screw of the microscope permits measurement of the vertical displacement. A relatively short horizontal length (≈ 20 microns) was used so that all measurements could be performed with the track centered in the field of view in order to eliminate errors arising from curvature-of-field effects. Again, caution was exercised not to be misled by scattering of the particle near the origin. In addition, a measure of pellicle thickness at the standard reference point was taken whenever dip angles were measured in a pellicle, because the "instantaneous" shrinkage factor must be known in order to calculate these angles. Two observers measured each event. A meaningful average error cannot be quoted for these observations, since the error is a function of the dip angle; all the measurements, however, were in reasonable agreement.

All the above angle measurements were performed on microscopes equipped with 10× oculars and 100× oil-immersion objectives.

CALCULATIONS

Range

The range of a given particle in a single pellicle is calculated in a straightforward fashion from the formula

$$R = \sum_i \{ (x_{i+1} - x_i)^2 + (y_{i+1} - y_i)^2 + [S(z_{i+1} - z_i)]^2 \}^{1/2} ,$$

where x_i, y_i, and z_i are the coordinates of a point on the track at which the ith measurement is taken, and S is the shrinkage factor for the prevailing relative humidity, i.e., the "instantaneous" shrinkage factor. If a particle traverses several pellicles, the individual pellicle ranges are summed to yield the total range. To facilitate range computations, a program that utilized the output of the automated microscope was written for the IBM 650 data-processing machine.

Since the range-energy relation is established for emulsion with the standard density 3.815 g/cc, corrections must be applied to ranges measured in emulsion of a different density. The range corrections in the 2B stack are of the order of 0.23% for the proton and 0.25% for the pion, and in the 2D stack, 0.49% and 0.54%. These figures are based upon Fig. 4 and upon the densities given in Table I. The energies corresponding to the corrected ranges are obtained from the range-energy relation for protons in emulsion of standard density.[14]

The statistical errors present in the range measurements are (a) measurement error and (b) range straggle. The measurement error, evaluated by carrying out two independent measurements on each track, was $\approx \pm 1/3\%$, as mentioned previously. In order to calculate an external statistical error for each event, it was assumed that a constant measurement error of $\pm 1/2\%$ applied to all range measurements. The magnitude of the second error, that of range straggle, is well known for emulsion and has been evaluated by Barkas et al.[15] for protons as a function of velocity. For a "typical" A event--i.e., one with a pion range ≈ 2.5 cm and a proton range

≈ 0.5 cm--the uncertainties introduced by range straggle are 3.2 % and 1.3% for the pion and proton, respectively. The range-straggle error is compounded with the measurement error to yield the total statistical error, which is used in the external-error calculation.

Various systematic errors are inherent in the range calculations, primary among these being the errors in measured emulsion density and in shrinkage factors. The fractional error in range arising from the uncertainty in emulsion density can be found by using the relation

$$\frac{\Delta R}{R} = K \left(\frac{\rho_m}{\rho_s}\right) \left(\frac{\Delta \rho_m}{\rho_m}\right),$$

where K is the percent range decrease per percent density increase, ρ_s the standard density, ρ_m the measured density, and $\Delta \rho_m$ the error in ρ_m. K is of the order of 0.8 for typical secondary ranges encountered in moderate-energy Λ decays. Note that the uncertainty in density, though small, is reflected almost directly into a range uncertainty of the same order of magnitude.

An uncertainty in the shrinkage factor produces a range error more difficult to evaluate generally, since the magnitude of the error is dependent upon the geometry of the track, i.e., the larger the Z component of range, the greater this error. On the assumption that the error in shrinkage factor was equal to its experimental error of ± 1 %, the range error was calculated explicitly for each track, and no general evaluation was attempted.

Space Angle

The space angle between the secondaries of a Λ-like event can be evaluated from the measured projected angle and dip angles by means of the formula

$$\cos \phi = \cos \delta_p \cos \delta_\pi (\tan \delta_p \tan \delta_\pi + \cos \theta) ,$$

where ϕ is the space angle, θ the projected angle, and δ_p and δ_π the dip angles of the proton and pion, respectively.

Measurement errors and multiple scattering of the secondaries give rise to a statistical error in the space-angle measurement. As mentioned previously, the projected angle was determined to within 0.4 deg. For the purpose of calculating an external statistical error, a constant error of $\pm 1/3$ deg was applied to all projected angle measurements and, when compounded with the statistical error arising from the multiple scattering of the proton, yielded the total statistical error in the projected angle, pion scattering being negligible. The magnitude of the proton multiple scattering as a function of velocity has been calculated for emulsion by Barkas and Young.[16]

Statistical error in the dip angles was assumed to result only from measurement error, the latter being large compared with the error introduced by scattering. However, no average statistical error can be cited for the dip-angle measurements, because the magnitude of the error depends upon the dip angle itself. Consequently, for each dip angle, the statistical error was taken to be the measurement error as determined from two independent observations.

With the aid of a program written for the IBM 650 data-processing machine, the space angle as well as its statistical error, evaluated from the total statistical errors in the dip and projected angles, was calculated for each event.

The space angle's only systematic error has its origin in the shrinkage-factor error of $\pm$ 1%, which introduces a systematic error in the dip-angle measurements.

MASS AND Q VALUE

The equations relating the mass and Q value of the Λ-hyperon in the decay $\Lambda \rightarrow p + \pi^-$ to the energies of the secondaries and to the space angle between them can be written

$$M_\Lambda = M_p \left[1 + \left(\frac{M_\pi}{M_p} \right) \left\{ \frac{M_\pi}{M_p} + 2 \left(\gamma_p \gamma_\pi - \sqrt{(\gamma_p^2 - 1)(\gamma_\pi^2 - 1)} \cos \phi \right) \right\} \right]^{1/2}$$

$$Q = M_\Lambda - (M_p + M_\pi) ,$$

where M_Λ, M_p, and M_π are the rest masses of the hyperon, proton and pion, respectively, γ_p and γ_π are the relativistic parameters for the proton and pion, and ϕ is the space angle.

By use of the first of the above relations, the mass and its total statistical error (which results from statistical errors in range and angle measurements) were evaluated for each event.

The distribution functions for the range and angle measurements of a given event are, of course, normal error curves with standard deviations equal to the measurement errors. If these errors are small, as they are here, they propagate linearly and the resulting distribution function for the mass value must be a normal error curve. Consequently, one can apply standard statistical procedures to calculate the mean value and its error.

The weighted means of the mass values, with the computed statistical error of each event used as the weighting factor, were determined for the two stacks; the results are:

2B stack: $M_\Lambda = 1115.30 \pm 0.11$ Mev (29 events),
2D stack: $M_\Lambda = 1115.46 \pm 0.08$ Mev (87 events).

The error quoted is the internal standard deviation of the mean. The mass-value ideogram for the 2B stack is shown in Fig. 5 and that for the 2D stack in Fig. 6. All events for which mass values differed from the mean by more than 2.5 standard deviations were considered background events. The 2B and 2D stacks contained six and five such events respectively, indicated in the ideograms by the shaded areas.

The internal and external errors were in very good agreement for the 2B stack. For the 2D stack, the internal error was 0.02 Mev greater than the external error; the discrepancy resulted from a broadening of the distribution because of the statistical fluctuation in the shrinkage factor, an effect not considered in the calculation of the total statistical error associated with each event. There is a difference, however, between the 2D stack and the 2B stack events; in the latter the secondaries lie predominantly in the plane of the emulsion, since presence of background hindered the detection of steep secondaries. Naturally, these "flat" events are less subject to errors in shrinkage factors; consequently, the above mentioned agreement between internal and external errors is to be expected if other undetected sources of error are absent.

Systematic errors for the mean values cited above were evaluated in the following manner: the uncertainty in the mass value of each event arising from a given systematic error was calculated explicitly; the systematic error in the mean value from this source equals the average of these mass uncertainties. The systematic errors include uncertainties in (a) the measured emulsion density, (b) the shrinkage factors, (c) the range-energy relation, and (d) the rest masses of the pion and proton. Table II lists the magnitudes of these errors and, for each stack, the resultant mean errors in the mean masses. The mass uncertainty resulting from the shrinkage-factor uncertainty differs for the two stacks because of the aforementioned difference in the geometries of the events in the stacks, i.e., 2B events are "flat" in comparison with the 2D events, which have almost all possible orientations.

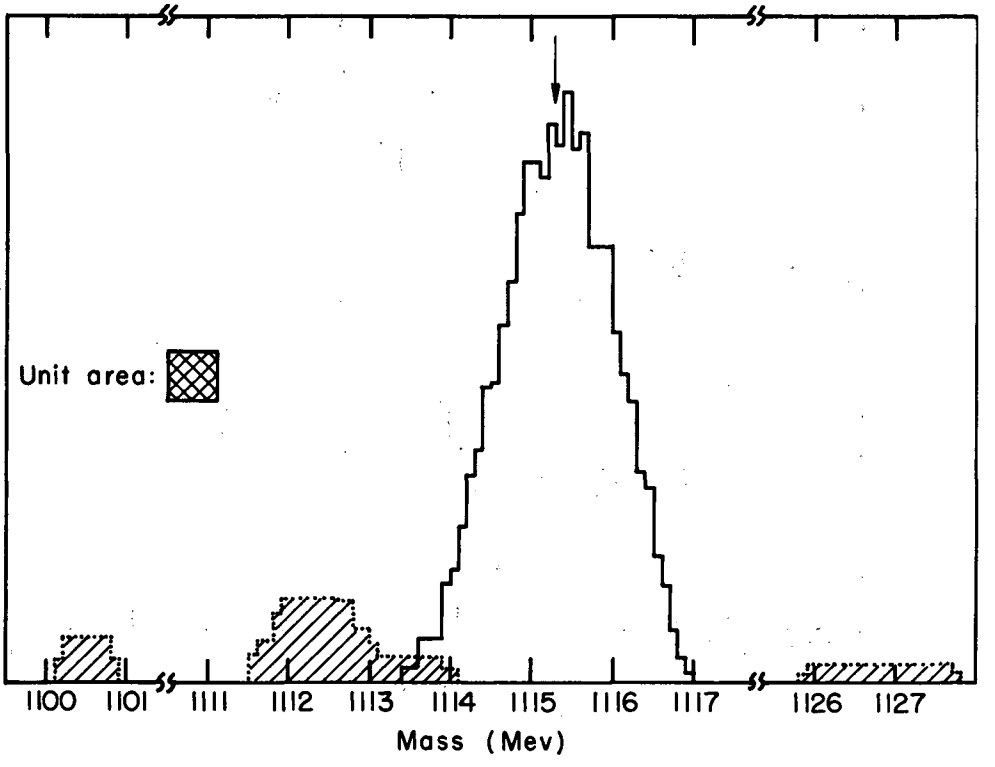

Fig. 5. Mass value ideogram for the 2B stack. The mean value, indicated by the arrow, is 1115.30 Mev; the statistical error in this result is ± 0.11 Mev (29 events). Shaded areas correspond to background events.

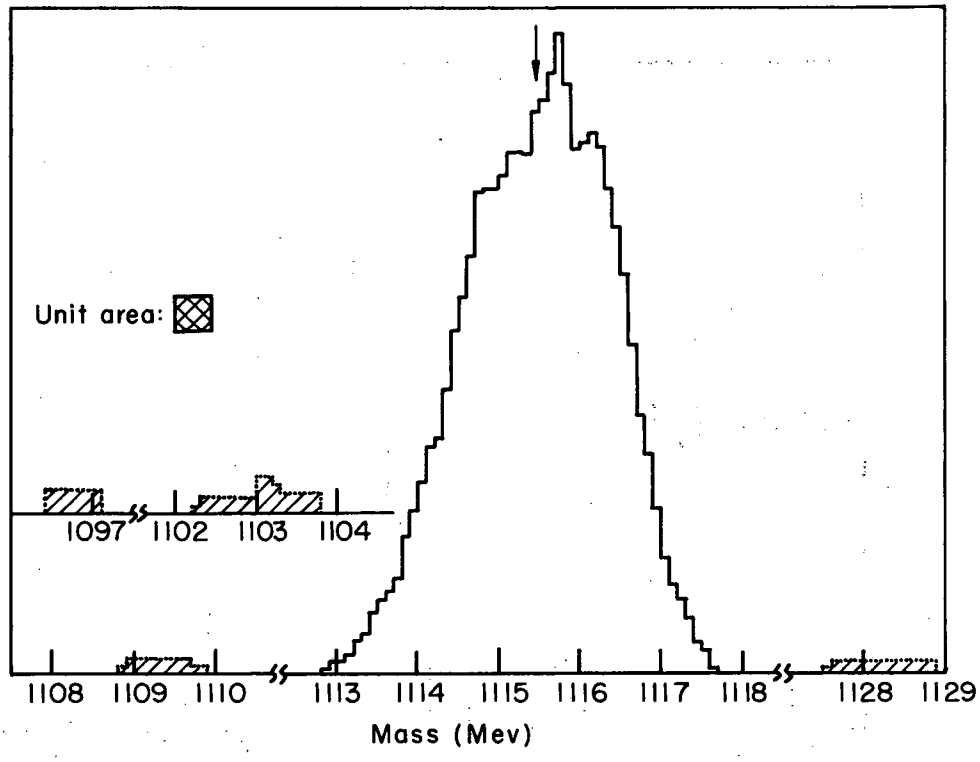

Fig. 6. Mass value ideogram for the 2D stack. The mean value, indicated by the arrow, is 1115.46 Mev; the statistical error in this result is ± 0.08 Mev (87 events). Shaded areas correspond to background events.

Table II

Source and magnitude of systematic error and the resulting mean errors in mean mass

Source	Magnitude of Error	Uncertainty in Mass (Mev)	
		2B Stack	2D Stack
(a) Emulsion density	~±0.1%[a]	±0.02	±0.01
(b) Shrinkage factors	±1.0%	±0.03	±0.04
(c) Range-Energy Relation	±0.5%	±0.11	±0.11
(d) Rest Energies			
Proton	±0.01 Mev	±0.01	±0.01
Pion	±0.06 Mev	±0.05	±0.05

[a] See Table I

Prior to calculation of a weighted mean mass for the two stacks, the systematic and statistical errors in mass associated with a stack must be compounded. These systematic errors, which become random in nature when a number of stacks are involved, are (a) the uncertainty in the emulsion density, and (b) the uncertainty in the shrinkage factors. Being now a combination of statistical, density, and shrinkage-factor errors, the total "statistical" uncertainty in the mean mass for the 2B stack remains ± 0.11 Mev, while for the 2D stack its value becomes ± 0.09 Mev. With these total errors, a comparison of the mean mass values for the two stacks shows no inconsistency. A χ^2 test indicates that one would expect two measurements to differ by at least this amount 28% of the time. Hence, a weighted mean can be obtained; it is M_Λ = 1115.40±0.07 Mev, and the Q value derived from this figure is 37.56±0.07 Mev.

The systematic errors introduced by uncertainties in the range-energy relation and the rest masses of the secondaries are combined with the above errors in the weighted mean mass and Q value to give the results (for 116 events):

$$M_\Lambda = 1115.40 \pm 0.14 \text{ Mev},$$
$$Q = 37.56 \pm 0.13 \text{ Mev}.$$

Normally, the error in Q value is less than that in mass as a result of smaller contributions from the rest-energy uncertainties of the secondaries, which are 0.01 Mev for the pion and nil for the proton.

Values for the proton and pion rest masses of 938.213±0.010 Mev and 139.63±0.06 Mev, respectively, were used.[17]

Most of the above computations were performed on the IBM 650 data-processing machine.

Three additional sources of error and their possible effects on the mean mass value must be considered. There are (a) pion inelastic scattering, (b) distortion of the emulsion, and (c) inner bremsstrahlung in the decay.

With regard to (a), the maximum energy loss that a pion could sustain without detectably altering a mass value would be approximately 2 Mev, since an event was considered background if its measured mass differed from the mean by more than 2.5 standard deviations. The probability of such an energy loss is very small. An undetected scattering, moreover, would have little effect on the mean mass; in fact, an event whose mass value is one standard deviation from the mean changes the 2B mean value by only 0.02 Mev and the 2D mean value by only 0.01 Mev.

The effects of emulsion distortion--which are not systematic in nature--are negligible, as demonstrated by the agreement of the internal and external statistical errors for each stack. This result is to be expected, since the region scanned for Λ-like events was in the central portion of each stack, the area most free from distortion. The pions of only a few 2D events approached the pellicle edges, where distortion may become severe, but these events did yield mass values within experimental errors. In addition, no large local distortions were observed in the course of area scanning.

An estimate of the effect of inner bremsstrahlung on the mean mass can be obtained by utilizing the semiclassical expression for the bremsstrahlung spectrum applied to the decay pion.[18] As in the case of inelastic pion scattering, the maximum photon energy must be limited to 2 Mev; a greater energy would result in the event's being classified as background. However, the average photon energy as calculated from the above spectrum with the imposed cutoff of 2 Mev is only 0.001 Mev--an amount which is completely negligible.

ENERGY SPECTRUM

The Λ-hyperon energy spectrum at production is a superposition of several spectra that arise from the allowed modes of Λ-hyperon production involving K^--meson reactions with complex nuclei. The types of reactions are:

(a) direct production with a single bound nucleon, e.g.,

$$K^- + N \rightarrow \Lambda + \pi;$$

(b) indirect production that involves the formation of an intermediate Σ hyperon, e.g., $K^- + N \rightarrow \Sigma + \pi$, followed by $\Sigma + N \rightarrow \Lambda + N$ and also by $\Sigma \rightarrow \Lambda + \gamma$ for the neutral Σ hyperon;

(c) direct production with two bound nucleons.

The reaction that gives rise to a particular Λ hyperon usually cannot be identified unambiguously because of the overlapping of the individual production spectra. However, if the effects of Λ-nucleon scattering are ignored, the energy spectrum at production can be obtained from the observed energy spectrum by correcting the latter for the geometry of the experiment. In addition, the absolute yield of "free" Λ hyperons--i.e., those not bound in hyperfragments--that are ultimately produced as a result of K^--meson reactions may be found. The results of an investigation whose aims were to determine the production spectrum and yield for a selected sample of events in the 2D stack are presented here.

In order to develop an expression that relates the production spectrum and yield to the experimentally observed quantities, one must make two assumptions. First, it is assumed that source space--the volume in which Λ-hyperon production occurs--is that region in which the K^- mesons react. In reality, the total source space includes not only this region but also the region in which the Σ-hyperon reactions take place. However, the geometries of the two source spaces are nearly identical, since, of the Σ hyperons that escape from the parent nuclei,

the charged hyperons typically travel about 7 mm before interaction, and the neutral hyperons--because of their fast radiative transition to Λ-hyperons--travel only negligible distances. In addition, charged-hyperon reactions contribute little to the Λ-hyperon flux; charged hyperons are emitted in approx. 18% of the K^--meson reactions,[19] and of this number, 60% decay.[20]

Second, to simplify the analytic treatment of this problem, Λ production from K^--meson reactions in flight was ignored. The angular distribution of the Λ-hyperons in observation space--a region much smaller than the total volume scanned for Λ-hyperons--showed no marked fore-aft asymmetry with respect to a plane normal to the beam direction. This neglect of in-flight interactions allows one to assume that Λ-hyperons are produced isotropically in reactions within source space.

The equation relating the yield and production spectrum to the observed energy spectrum and the total number of decays is

$$\frac{a g(r_0)}{4\pi r_0} \int_V \int_{V'} \rho(x', y', z')\, e^{-r/r_0}\, \frac{1}{r^2}\, dV' dV = N_0 g_0(r_0), \tag{1}$$

where $a g(r_0)$ is the probability of producing a Λ-hyperon whose mean decay length in the laboratory system is r_0 (where $r_0 = \gamma\beta c\tau$); $\rho(x', y', z')$ is the density of K mesons in source space; $r = \{ (x'-X)^2 + (y'-Y)^2 + (z'-Z)^2 \}^{1/2}$, the distance between the volume element dV' in source space and the volume element dV in observation space; N_0 is the total number of hyperons found in observation space; and $g_0(r_0)$ is the observed spectrum. The location of the origin of the coordinate system to which a point x', y', z' in source space and a point X, Y, Z in observation space are referred is arbitrary. The equation may be written in the above form, because there is no correlation between the hyperon production energy and its

point of production in source space, i. e., the production distribution function of Λ-hyperons in source space is given by $ag(r_0)\rho(x', y', z')$. For convenience, let $I(X, Y, Z, r_0)$ denote the integration over source space, and $J(r_0) = \int_V I(X, Y, Z, r_0)\, dV$. Then,

$$ag(r_0) = 4\pi N_0 g_0(r_0) r_0 / J(r_0), \tag{2}$$

so that the yield is given by

$$a = a \int_0^\infty g(r_0)\, dr_0 = 4\pi N_0 \int_0^\infty \{ g_0(r_0) \cdot r_0 / J(r_0) \}\, dr_0 . \tag{3}$$

The evaluation of I and J proves difficult for any but the simplest geometries. In our case, it is found that the density of the K^- mesons is well represented by the function

$$\rho = \rho_0 \exp \left\{ -\frac{1}{2} \left[\left(\frac{x'}{\sigma_{x'}}\right)^2 + \left(\frac{y'}{\sigma_{y'}}\right)^2 + \left(\frac{z'}{\sigma_{z'}}\right)^2 \right] \right\} , \tag{4}$$

i. e., the product of three normal distributions, where the x' axis is taken along the beam direction, the y' axis is the vertical, and the z' axis is the horizontal; $\sigma_{x'} = 7.2$ mm, $\sigma_{y'} = 11.8$ mm, $\sigma_{z'} = 20.9$ mm, and $\rho_0 = 300$ K^- mesons/cc. The origin of the coordinate system is taken to be at the center of source space so that ρ_0 represents the density of stars at the origin.

The evaluation of I can be performed by transformation to a coordinate system centered at the point X, Y, Z. Algebraic operations applied to the integrand, in which the explicit function of the density appears, yield

$$I(X, Y, Z, r_0) = \rho_0 e^{-\gamma_0} \int_0^{2\pi} \int_0^{\pi} \int_0^{\infty} \exp\left\{\frac{1}{4} \frac{\left(\gamma_1 + \frac{1}{r_0}\right)^2}{\gamma_2}\right\} \exp\left\{-\gamma_2 \left[r + \frac{\left(\gamma_1 + \frac{1}{r_0}\right)}{2\gamma_2}\right]^2\right\} dr \sin\theta \, d\theta \, d\phi, \quad (5)$$

where

$$\gamma_0(X, Y, Z) = \frac{1}{2}\left[\left(\frac{X}{\sigma_{x'}}\right)^2 + \left(\frac{Y}{\sigma_{y'}}\right)^2 + \left(\frac{Z}{\sigma_{z'}}\right)^2\right],$$

$$\gamma_1(X, Y, Z, \theta, \phi) = \left[\frac{X \sin\theta \cos\phi}{\sigma_{x'}^2} + \frac{Y \sin\theta \sin\phi}{\sigma_{y'}^2} + \frac{Z \cos\theta}{\sigma_{z'}^2}\right],$$

$$\gamma_2(\theta, \phi) = \frac{1}{2}\left[\left(\frac{\sin\theta \cos\phi}{\sigma_{x'}}\right)^2 + \left(\frac{\sin\theta \sin\phi}{\sigma_{y'}}\right)^2 + \left(\frac{\cos\theta}{\sigma_{z'}}\right)^2\right],$$

which, upon integration over r, can be written as

$$I(X, Y, Z, r_0) =$$

$$\rho_0 e^{-\gamma_0} \int_0^{2\pi} \int_0^{\pi} \exp\left\{\frac{1}{4} \frac{\left(\gamma_1 + \frac{1}{r_0}\right)^2}{\gamma_2}\right\} \frac{1}{\sqrt{\gamma_2}} \left\{\frac{\sqrt{\pi}}{2} - \sum_{m=0}^{\infty} \frac{(-1)^m}{(m!)(2m+1)} \left[\frac{\left(\gamma_1 + \frac{1}{r_0}\right)}{2\sqrt{\gamma_2}}\right]^{2m+1}\right\} \sin\theta \, d\theta \, d\phi. \quad (6)$$

No analytical evaluation of the integration over the angles was attempted; instead, an approximate result was obtained by (a) determining, for a given r_0, the values of the integrand at the point X, Y, Z in the positive and negative directions of the coordinate axes of the translated coordinate system, (b) averaging these, and (c) integrating the average value--denoted by $G(X, Y, Z, r_0)$--over the whole solid angle. The error

introduced by this approximation is approx 11%. If the maximum values of X, Y, and Z are limited to $\sigma_{x'}$, $\sigma_{y'}$, and $\sigma_{z'}$, respectively, then--to ±8%--G is independent of X, Y, and Z for values of r_0 encountered in this experiment, excluding the very small ($r_0 < 1/2$ cm) and the very large ($r_0 > 3$ cm). Consequently, the evaluation of J is easily performed, since $I(r_0)$ becomes simply $4\pi\rho_0 e^{-\gamma_0} G(r_0)$; thus

$$J(r_0) = 4\pi\, G(r_0) \int_V \rho_0\, e^{-\gamma_0}\, dV$$

$$= 4\pi\, G(r_0) \int_V \rho\,(X, Y, Z)\, dV$$

$$= 4\pi\, G(r_0)\, N_K\,,$$

where N_K is the number of K mesons contained in observation space. Hence

$$a\, g(r_0) = \left(\frac{N_0}{N_K}\right) g_0(r_0)\, \frac{r_0}{G(r_0)} \tag{7}$$

and

$$a = \frac{N_0}{N_K} \int_0^\infty g_0(r_0)\, \frac{r_0}{G(r_0)}\, dr_0\,. \tag{8}$$

The following boundaries were given to observation space (the region systematically searched for Λ hyperons): $-\sigma_{x'} \leqslant X \leqslant \sigma_{x'}$, $-\sigma_{y'} \leqslant Y \leqslant \sigma_{y'}$, $-0.35\,\sigma_{z'} \leqslant Z \leqslant +0.8\,\sigma_{z'}$.

In order to evaluate the absolute yield it is necessary to determine the efficiencies of those who scanned for Λ-like events. Reliable data of this nature are limited to a small percentage of the personnel so engaged and these found a total of 17 Λ hyperons, or 30% of the total number in observation space. A yield determination based on such small numbers would have little meaning, the minimum uncertainty being at least ± 25%. As a result, only a geometric correction is applied to the observed spectrum.

As mentioned above, $G(X, Y, Z, r_0)$ is not independent of X, Y, and Z for small values of r_0. This behavior stems from the divergent nature of the integrand as r_0 tends to zero, as is evident from an inspection of Eq. (6). However, one can show that the geometric correction factor--r_0/G--approaches unity as r_0 approaches zero as follows: if r_0 is small, only the local density of K mesons in the vicinity of the point X, Y, Z becomes important, since $\exp[-(r/r_0)]$ is large only for small values of r. Consequently,

$$\rho(x', y', z') \approx \rho(X, Y, Z),$$

so that

$$I(X, Y, Z, r_0) \approx \rho(X, Y, Z) \int_{V'} e^{-r/r_0} \cdot \frac{1}{r^2}\, dV' \approx 4\pi r_0 \rho(X, Y, Z) .$$

Thus

$$J(r_0) \approx 4\pi r_0 \int_V \rho(X, Y, Z)\, dV \approx 4\pi r_0 N_K$$

and

$$\alpha g(r_0) \approx \left(\frac{N_0}{N_K}\right) g_0(r_0) , \qquad (9)$$

which corresponds to the previous result (see Eq. (7)) if r_0/G is set equal to unity.

The values of r_0/G as a function of hyperon energy as well as the observed and corrected spectra appear in Fig. 7.

Only those Λ-like events were analyzed in which the decay secondaries came to rest. Thus, a possible bias in the observed distribution arises from the effect of π^- interactions in flight. The magnitude of the correction factor that compensates for this effect can be estimated by assuming that the interaction cross section is independent of energy and equal to the geometric cross section. Because the number of high-energy hyperons--those in the interval from 25 Mev to 50 Mev--is small, the correction to be applied to this portion of the spectrum is also small (one event) and can be neglected in view of the large statistical errors in this region. For the remaining events of lower energy, virtually no correlation exists between the kinetic energies of the decay pion and the Λ hyperon. If one assumes a mean pion range ≈ 2.1 cm for these events, a total of three events should be added to the observed spectrum, again a small correction. A total of four Λ-like events whose decay pions did interact in flight was observed. Pions that escape from the stack constitute an additional source of bias. Although observation space was centrally located in the stack, where the probability of escape was small, one such event was observed. A correction of only one event has no influence on the observed spectrum within statistical errors. Finally, one must consider the effect of scanning efficiencies that depend upon the momenta of the Λ hyperons. No reliable data are available to correct for such an effect, if indeed it exists.

A similar determination of the Λ-hyperon production spectrum has been performed by Bogdanowicz et al., who used Monte Carlo techniques to calculate for their observed spectrum a correction factor, which is only partially geometric in nature.[21]

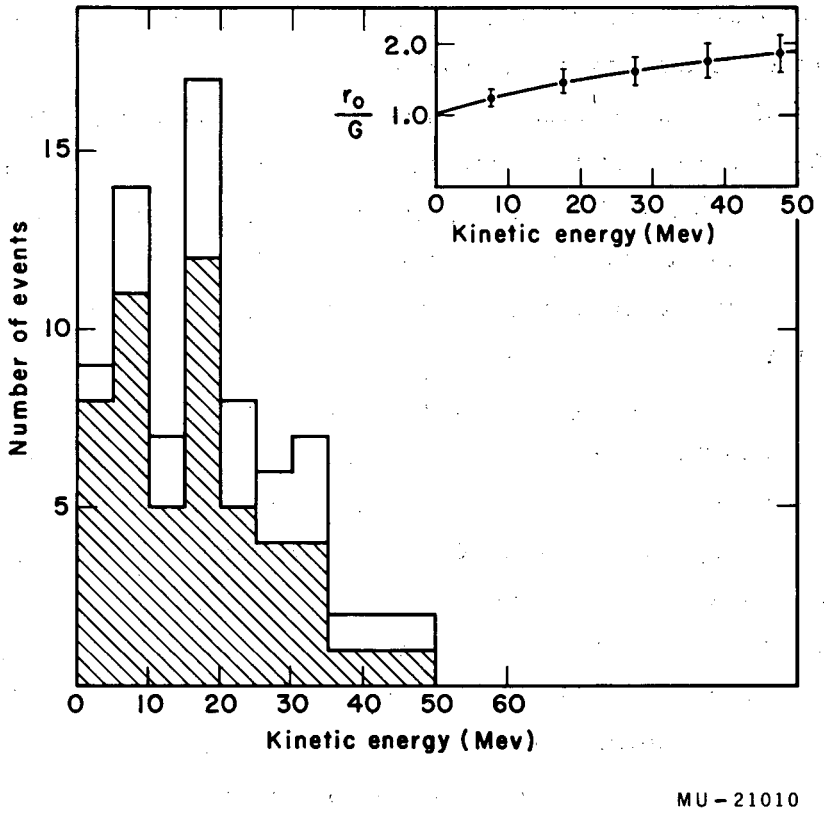

Fig. 7. Energy spectrum of Λ hyperons. The unshaded histogram corresponds to the corrected spectrum, the shaded histogram to the observed spectrum. The geometric correction factor, shown in the inset, is plotted as a function of hyperon energy.

ACKNOWLEDGMENTS

I am indebted to Dr. Walter H. Barkas for having suggested this research program and for his helpful guidance. I am grateful to Dr. Robert L. Thornton for his interest and encouragement.

My sincere thanks to the scanners who found the events and assisted in the measurements, particularly to Miss Ernestine Beleal and Mrs. Hester Yee, who performed the range measurements.

I wish to thank Mrs. Penny Vedder for programming the energy-spectrum correction-factor calculation and assisting in the machine computations.

My sincere appreciation to Mr. James C. Hodges for the construction of the automated microscope and to Mr. Thomas Taussig for the design of the associated electronics.

My appreciation also is due the members of the Barkas physics research group, the Bevatron crew, and all the many people who helped developed the K^--meson beams and assisted in the exposures.

Finally, my deepest appreciation to my wife, Mary Ellen, for her continued enthusiasm and encouragement.

This work was done under the auspices of the U. S. Atomic Energy Commission.

APPENDIX

Automated Microscope

The microscope has long been the basic tool for research that employs nuclear emulsion techniques. Successive refinements in mechanical design have produced instruments noteworthy for their precision. However, to make full use of their capabilities has always meant the devotion of much time to the routine task of "dial-reading."

With the development of devices that ascertain and express electrically the angular position of a shaft, measurements performed on a microscope now can be carried out quickly, yet with a precision comparable to that obtainable from a standard research microscope. Known as analog-to-digital converters ("digitizers"), these devices transform shaft position into a discrete combination of on-off switches by means of a coded-disk and wiper-arm assembly. A microscope equipped with these converters and the associated electronic equipment forms a complete system for the automatic readout of the X, Y, and Z coordinates of any point in the "working volume" of the instrument.[22] The output of this system may be channeled into various devices for data presentation, but preferably should employ one that can introduce information into a computer.

A system of this form has been in almost continuous use for two years. As expected, an over-all reduction in time spent upon taking measurements is effected; typically, range measurements on particles that traverse several pellicles are performed at a rate five times as fast as when employing manual techniques--without loss of precision. Simultaneously, the elimination of "dial-reading" error increases the reliability of the measurements. Also, the acquisition of the data in a form suitable for processing by high-speed computers has proved advantageous for the problem of data reduction.

The microscope in use--pictured in Figs. 8 and 9--has been specifically designed to solve the problem of scanning large emulsion pellicles.[23] A large stage allows for the adequate support of these pellicles in almost any orientation. Lead screws with travels of 10 cm on both the X and Y axes allow coverage of a wide area, eliminating much of the need for plate relocation. A novel feature of the design, suggested by Dr. Harry H. Heckman, is the split yoke used to support a standard binocular head. A 13-in. clearance between the objective and the yoke at the stage level is achieved without sacrificing structural rigidity. This assembly proves more rigid than the ordinary microscope, which has a very limited throat capacity. Further, this design allows the inclusion of a suitable illuminating source without the problems that arise from the need for thermal isolation of the light source and, most important, from the necessity of obtaining a good image.

Of the analog-to-digital converters attached to the three mechanical axes of this microscope, those on the X and Y screws yield 1000 counts per revolution for 100 revolutions. As a result, with the millimeter-per-revolution pitch of the screws on these movements, the least distance measurable is 1 micron anywhere in an interval of 10 cm. The Z axis is equipped with a thousand-count-per-revolution unit, which is limited to one revolution. Using a 10-to-1 reduction between the disk and the fine-focus screw, one can measure vertical distances of 1 μ anywhere in an interval of 1 mm.

The associated electronic equipment performs a variety of functions, as illustrated schematically in Fig.10. First, because the output of the digitizers is in binary form, it must be converted to decimal form before card-punching, this conversion being performed by a translator. The three disks are read sequentially into the translator, whose output is fed into a card punch via a punch-control chassis.

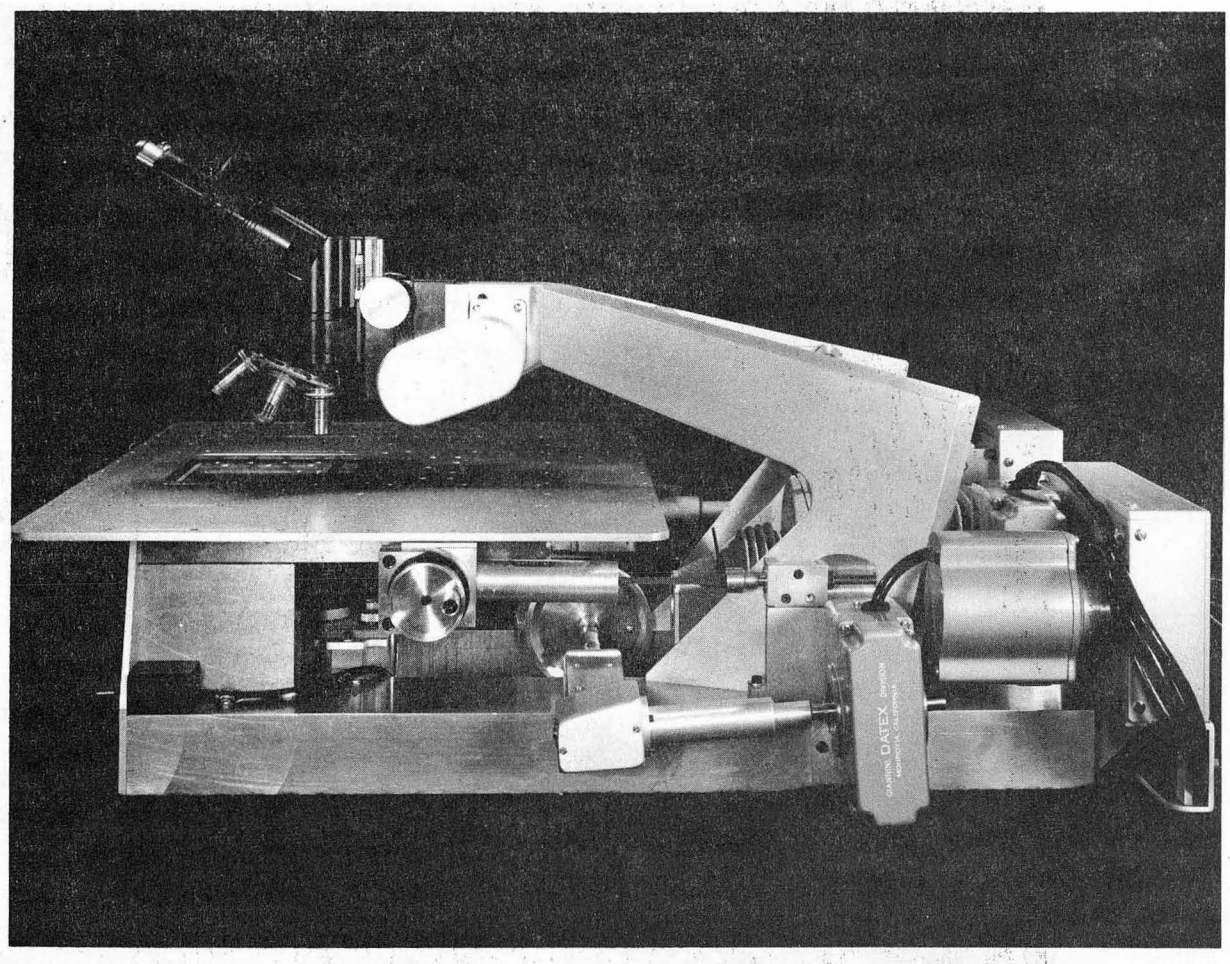

ZN-2441

Fig. 8. Side view of automated microscope. The encoder assemblies are mounted at the rear of the instrument.

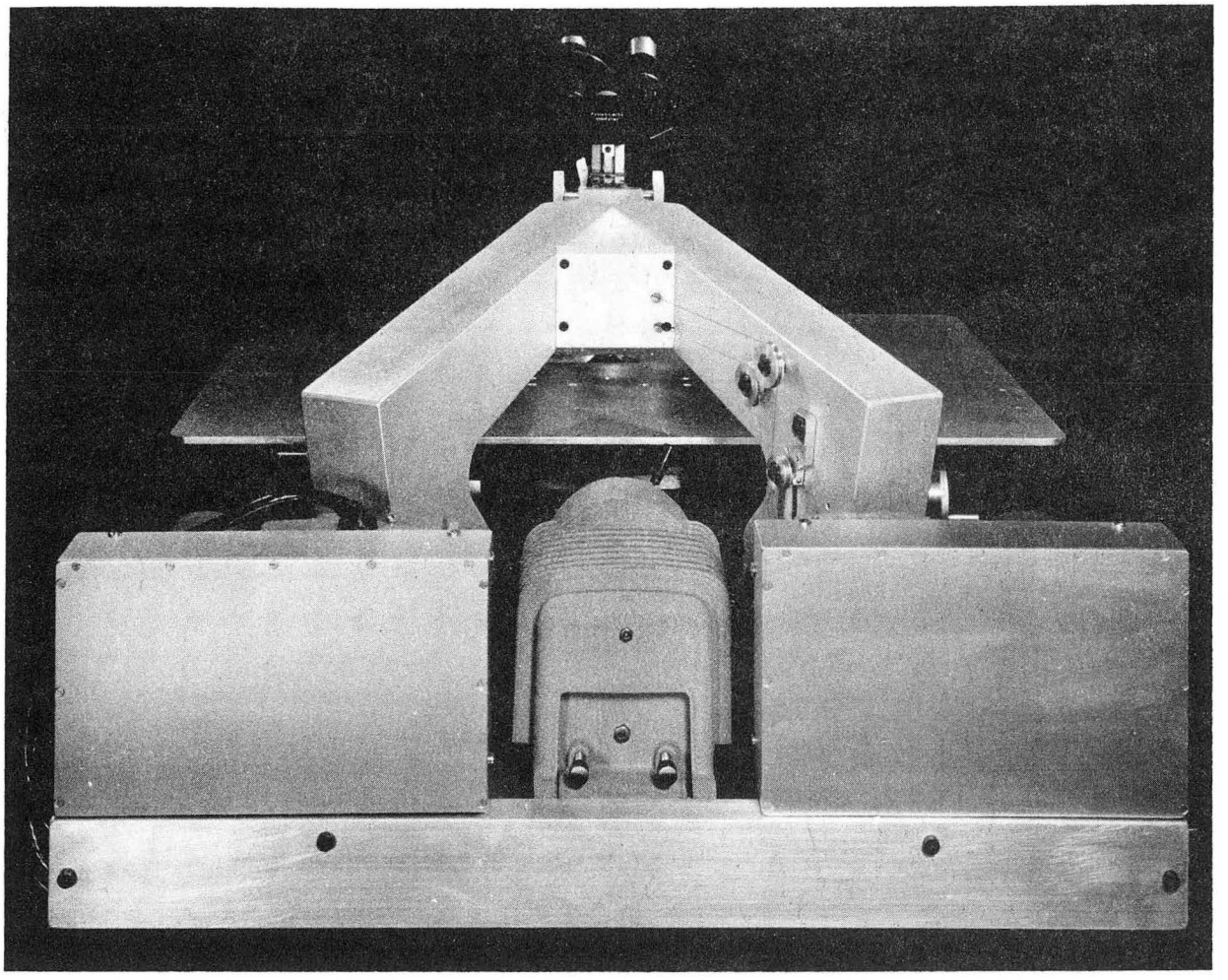

ZN-2442

Fig. 9. Rear view of the automated microscope, showing the split yoke and location of the illuminator.

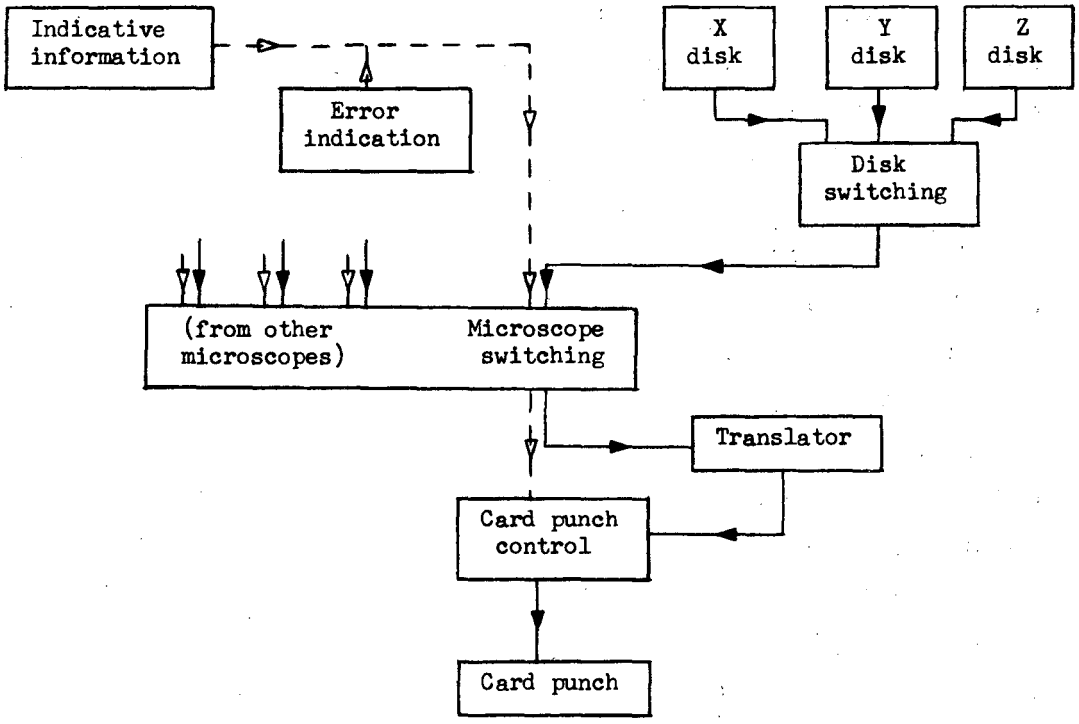

Fig. 10. Information flow diagram. The paths of the indicative information and of the coordinate information are represented by the dotted and solid lines, respectively.

Second, because punched cards form the raw data, it is desirable to punch indicative information on each card to identify it. Thus, in addition to the three coordinates associated with a particular point, the following information appears: (a) event number, (b) prong number, (c) pellicle number, (d) microscope number, and (e) card number (entered automatically). The entry of this information on the cards is accomplished electronically by an indicative-information control panel, shown in Fig. 11.

Third, in any system of this sort, a provision for correcting errors in measurement is essential. Suitable computer programming can detect the presence of an error-identification punch and negate the effect of the error. Circuitry providing for the insertion of such a punch is included.

Fourth, provision has been made for expansion of the system to accommodate a greater number of microscopes, while still using only one translator, one punch-control chassis, and one card punch. Suitable interlocking circuitry can be incorporated in a microscope-switching chassis to prevent the simultaneous entry of data from different microscopes. Each additional microscope will require for information entry, only the three digitizers, the indicative-information control panel, and a disk-switching chassis. The system was designed in this manner because with an automated microscope more time would be spent in the operations of track-following than in data recording (in marked contrast to manual readout methods). If limited to a single microscope, the circuitry and card punch would stand idle most of the time, but by having several microscopes work into a punch and "common" electronics, a more efficient duty cycle is obtained.

The bulk of the circuitry is reduced by the use of transistors and printed-circuit boards, both of which also serve to reduce maintenance problems. Relatively "fast" circuitry is employed to keep readout time to a minimum. As a result, the time required to punch the indicative information and the three coordinates is 4 seconds, the maximum speed of the card punch.

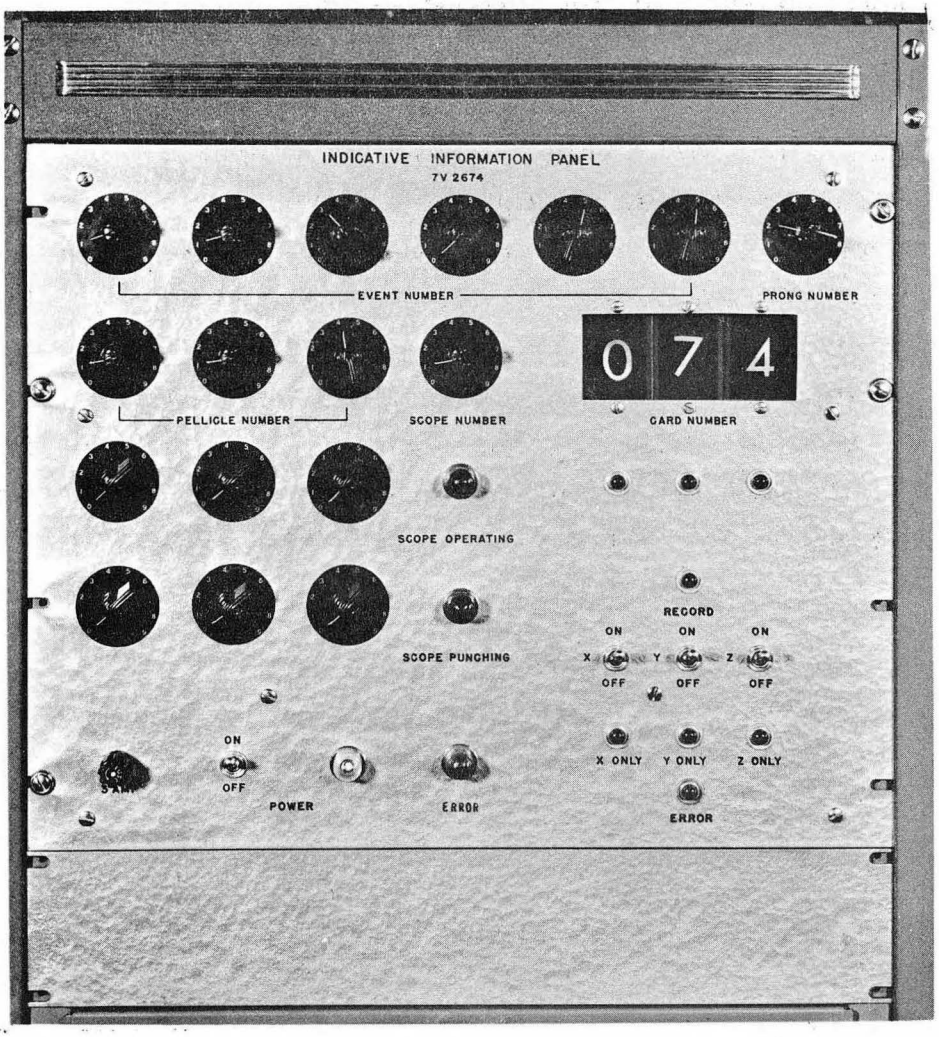

ZN-2031

Fig. 11. Indicative information control panel, showing the arrangement of the rotary switches used to enter the indicative information. The control switches are on the lower right.

Considerable attention was paid to the problem of providing a system easily used by scanning personnel. In actual practice, one need perform only two operations when measuring an event (after initially setting the rotary switches on the indicative-information control panel): (a) depressing the "record" button when a measurement is taken, and (b) resetting the pellicle-number switches as a particle traverses successive pellicles. There is no need to signify the end of an event or attend to the card numbering; nor is there any necessity to operate the microscope any differently from the ordinary research microscope. For convenience, the "record" and "error" switches located on the indicative-information control panel are duplicated in function by similar switches in a small box situated near the microscope; a foot switch is also provided which serves as an alternative "record" switch.

REFERENCES

1. G. D. Rochester and C. C. Butler, Nature 160, 855 (1947).
2. R. W. Thompson, in Progress in Cosmic Ray Physics, Vol. 3, (North-Holland Publishing Co., Amsterdam, 1956), Chapter III.
3. M. W. Friedlander, D. Keefe, M. G. K. Menon, and M. Merlin, Phil. Mag. 45, 533 (1954).
4. M. Danysz and J. Pniewski, Phil. Mag. 44, 348 (1953).
5. V. L. Telegdi, in Proceedings of the Seventh Annual Rochester Conference on High Energy Nuclear Physics, (Interscience Publishers, Inc., New York, 1957), p. VIII-6.
6. R. Armenteros as quoted by L. Alvarez, in Proceedings of the Seventh Annual Rochester Conference on High Energy Nuclear Physics (Interscience Publishers, Inc., New York, 1957) p. VI-3; also
   C. D'Andlau, R. Armenteros, A. Astier, H. C. DeStaebler, B. P. Gregory, L. Leprince-Ringuet, F. Muller, C. Peyrou, and J. H. Tinlot, Nuovo cimento 6, 1135 (1957).
7. H. H. Heckman, F. W. Inman, C. J. Mason, N. A. Nickols, F. M. Smith, W. H. Barkas, W. F. Dudziak, and P. C. Giles, Enriched K-Meson Beams from the Bevatron, UCRL-3549, Oct. 1956.
8. W. H. Barkas, P. C. Giles, H. H. Heckman, F. W. Inman, C. J. Mason, and F. M. Smith, Padua-Venice Conference Report, (1957) p. VI-41.
9. J. Bogdanowicz, M. Danysz, A. Filipkowsky, E. Marquit, E. Skrzypczak, A. Wroblewski, and J. Zakrzewski, Nuovo cimento 11, 727 (1959).
10. R. Ammar, R. Levi Setti, W. E. Slater, S. Limentani, P. E. Schlein, and P. H. Steinberg, Nuovo cimento 15, 181 (1960).

11. Joseph J. Murray, A Coaxial Static-Electromagnetic Velocity Spectrometer for High-Energy Particles, UCRL-3492, May 1957.
12. N. Horwitz, J. J. Murray, R. R. Ross and R. D. Tripp, 450-Mev/c K^- and $\bar{p}$ Beams at the Northwest Target Area of the Bevatron Separated by the Coaxial Velocity Spectrometer, UCRL-8269, June 1958.
13. W. H. Barkas, P. H. Barrett, P. Cüer, H. Heckman, F. M. Smith, and H. K. Ticho, Nuovo cimento 8, 185 (1958).
14. W. H. Barkas, Nuovo cimento 8, 201 (1958).
15. W. H. Barkas, F. M. Smith, and W. Birnbaum, Phys. Rev. 98, 605 (1955).
16. W. H. Barkas and D. M. Young, Emulsion Tables. I. Heavy-Particle Functions, UCRL-2579 Rev., Sept. 1954.
17. W. H. Barkas and A. H. Rosenfeld, Data for Elementary-Particle Physics, UCRL-8030 Rev., July 1959.
18. Wolfgang K. H. Panofsky and Melba Phillips, Classical Electricity and Magnetism (Addison-Wesley Publishing Co., Inc., Massachusetts, 1955), p. 305.
19. Y. Eisenberg, W. Koch, M. Nikolić, M. Schneeberger, and H. Winzeler, Nuovo cimento 11, 351 (1959).
20. John N. Dyer (Lawrence Radiation Laboratory), private communication.
21. J. Bogdanowicz, A. Filipkowski, A. Krzywicki, E. Marquit, E. Skrzypczak, A. Wróblewski and J. Zakrzewski, A Method for Determination of the Energy Spectrum of Λ Hyperons in K^- Interactions with Emulsion Nuclei, Polish Academy of Sciences - Institute of Nuclear Research Report No. 107/VI, Sept. 1959.
22. C. J. Mason and W. H. Barkas, A Microscope with Automatic Coordinate Readout Adapted for Calculating Particle Ranges, UCRL-8306 Abstract, May 1958.
23. J. C. Hodges, A Deep-Throat Digitized Microscope, UCID-955, Oct. 1958.